AFRL-AFOSR-UK-TR-2011-0030

On the Evolution of Vortical Disturbances in Two-Fluid Boundary Layers

Tamer A. Zaki

Imperial College London
Department of Mechanical Engineering
Exhibition Road
London, United Kingdom SW7 2AZ

EOARD GRANT 09-3059

July 2011

Final Report for 18 March 2009 to 18 March 2011

Distribution Statement A: Approved for public release distribution is unlimited.

Air Force Research Laboratory
Air Force Office of Scientific Research
European Office of Aerospace Research and Development
Unit 4515 Box 14, APO AE 09421

REPORT DOCUMENTATION PAGE

Form Approved OMB No. 0704-0188

Public reporting burden for this collection of information is estimated to average 1 hour per response, including the time for reviewing instructions, searching existing data sources, gathering and maintaining the data needed, and completing and reviewing the collection of information. Send comments regarding this burden estimate or any other aspect of this collection of information, including suggestions for reducing the burden, to Department of Defense, Washington Headquarters Services, Directorate for Information Operations and Reports (0704-0188), 1215 Jefferson Davis Highway, Suite 1204, Arlington, VA 22202-4302. Respondents should be aware that notwithstanding any other provision of law, no person shall be subject to any penalty for failing to comply with a collection of information if it does not display a currently valid OMB control number.
PLEASE DO NOT RETURN YOUR FORM TO THE ABOVE ADDRESS.

1. REPORT DATE *(DD-MM-YYYY)*	2. REPORT TYPE	3. DATES COVERED *(From – To)*
26-07-2011	Final Report	18 March 2009 – 18 March 2011

4. TITLE AND SUBTITLE

On the Evolution of Vortical Disturbances in Two-Fluid Boundary Layers

5a. CONTRACT NUMBER

FA8655-09-1-3059

5b. GRANT NUMBER

Grant 09-3059

5c. PROGRAM ELEMENT NUMBER

6. AUTHOR(S)

Dr. Tamer A. Zaki

5d. PROJECT NUMBER

5d. TASK NUMBER

5e. WORK UNIT NUMBER

7. PERFORMING ORGANIZATION NAME(S) AND ADDRESS(ES)

Imperial College London
Department of Mechanical Engineering
Exhibition Road
London, United Kingdom SW7 2AZ

8. PERFORMING ORGANIZATION REPORT NUMBER

N/A

9. SPONSORING/MONITORING AGENCY NAME(S) AND ADDRESS(ES)

EOARD
Unit 4515 BOX 14
APO AE 09421

10. SPONSOR/MONITOR'S ACRONYM(S)

AFRL/AFOSR/RSW (EOARD)

11. SPONSOR/MONITOR'S REPORT NUMBER(S)

AFRL-AFOSR-UK-TR-2011-0030

12. DISTRIBUTION/AVAILABILITY STATEMENT

Approved for public release; distribution is unlimited.

13. SUPPLEMENTARY NOTES

14. ABSTRACT

Boundary layer stability, and the ability to maintain a laminar flow near the wall, are compromised in presence of free-stream vortical forcing. The low-frequency free-stream disturbances penetrate boundary layer despite the sheltering ability of the mean shear. These disturbances form streaks via the lift-up mechanism. The streaks subsequently become unstable and breakdown to turbulence. The stability of laminar boundary layers is examined in presence of a thin wall-film, of different viscosity. The influence of the film on the evolution of free-stream vortical modes and the generation of boundary layer streaks is solved analytically. It is shown that a lower viscosity film can reduce the transient amplification due to the lift-up mechanism, and hence enhance the flow stability. However, the presence of the wall-film also introduces a new mechanism for the generation of normal vorticity. This mechanism become dominant when the viscosity of the lower film is reduced below a critical level. The results from the linear analysis are complemented by direct numerical simulations which take into account non-parallel and non-linear effects, e.g. finite displacement of the two-fluid interface.

15. SUBJECT TERMS

EOARD, Aerodyanamics, Transition, Boundary Layer

16. SECURITY CLASSIFICATION OF:			17. LIMITATION OF ABSTRACT	18, NUMBER OF PAGES	19a. NAME OF RESPONSIBLE PERSON
a. REPORT	b. ABSTRACT	c. THIS PAGE			Gregg Abate
UNCLAS	UNCLAS	UNCLAS	SAR	22	19b. TELEPHONE NUMBER *(Include area code)* +44 (0)1895 616021

Standard Form 298 (Rev. 8/98)
Prescribed by ANSI Std. Z39-18

On the evolution of vortical disturbances in two-fluid boundary layers

Contract FA8655-09-1-3059†
Final report
March 2011

† This report was prepared in fulfilment of the final deliverable for contract FA8655-09-1-3059, based on the work of Dr. T. A. Zaki (t.zaki@imperial.ac.uk), S. Saha and S.Y. Jung.

CONTENTS

1. Introduction **4**
1.1. The continuous spectrum 4
1.2. The amplification of streaks 6

2. Linear analysis **7**
2.1. The base flow 7
2.2. The linear perturbation equations 8
2.3. The solution of the initial value problem 9

3. Evaluation of the boundary layer response to vortical forcing **11**
3.1. Viscosity stratification effects 13

4. Direct numerical simulations **15**
4.1. The numerical method 15
4.2. Numerical results 16

5. Conclusions **18**

List of figures

1 Effect of ω on penetration depth $(R = 1000, k_z = \pi, k_y = \pi)$, —— $\omega = \pi$, - - - $\omega = \pi/10$, — · — $\omega = \pi/100$. 5

2 High frequency oscillations in mode shape for an extremely dense film. ——, real component; - - -, imaginary component. $k_x Re_T = 1/100, k_y = \pi/4, k_z = \pi, \delta_B = 0.3, \rho_{BT} = 1000$. Note, ϕ is plotted on separate scales in the top and bottom fluids 5

3 Variation of penetration depth with viscosity ratio where $k_x Re_T = \frac{1}{100}, k_y = \frac{\pi}{4}, k_z = \pi$, $\circ$ $\delta_B = 0.3$, $\triangle$ $\delta_B = 0.2$ 6

4 Schematic of a two-fluid boundary layer under the influence of a continuous mode and an interface mode. 7

5 Projection of forcing $|\kappa| \equiv |\langle \hat{\mathcal{X}}^{\dagger}_{\bar{k},k_y}, \mathscr{F} \rangle|$ on the homogeneous Squire eigenfunctions. ——, interfacial mode; - - -, continuous Orr–Sommerfeld mode. The forcing mode has $\omega_{int} = 0.000373$, $k_x = 0.001$, $k_{y,cont} = \pi$, $k_z = \pi$ and the Reynolds number is $Re = 800$. The film thickness and viscosity are $d = 0.1$ and $\mu_{BT} = 0.3$. 12

6 (a) Normal velocity and (b) interface displacement at different instants of time. ——, $t = 0$; - - -, $t = 44$; — · —, $t = 314$. The forcing mode has $\omega_{int} = 0.000373$, $k_x = 0.001$, $k_{y,cont} = \pi$, $k_z = \pi$ and the Reynolds number is $Re = 800$. The film thickness and viscosity are $d = 0.1$ and $\mu_{BT} = 0.3$. . 12

7 (a) Normal vorticity response at different instants in time, ——, $t = 0$; - - -, $t = 44$; — · —, $t = 314$. A zoomed in view of the boundary layer is shown in pane (b). The forcing mode parameters are $\omega_{int} = 0.000373$, $k_x = 0.001$, $k_{y,cont} = \pi$, $k_z = \pi$ and the Reynolds number is $Re = 800$. The film thickness and viscosity are $d = 0.1$ and $\mu_{BT} = 0.3$. 13

8 Squire response in a two-fluid boundary layer at the time of maximum amplification in energy. $d = 0.1$ ——, $\mu_{BT} = 1.0$; · · · ·, $\mu_{BT} = 0.5$; — · —, $\mu_{BT} = 0.3$; - - -, $\mu_{BT} = 0.2$. $k_x = 0.001, k_y = \pi, k_z = \pi, Re = 800$ 13

9 (a)Tilting term, $|d_y U \phi|$ for a two-fluid boundary layer (b) Tilting term, $|d_y U \phi|$ inside the boundary layer. $d = 0.1$ ——, $\mu_{BT} = 1.0$; · · · ·, $\mu_{BT} = 0.5$; — · —, $\mu_{BT} = 0.3$; - - -, $\mu_{BT} = 0.2$. $k_x = 0.001, k_y = \pi, k_z = \pi, Re = 800$. 14

10 Coupling coefficient contours, θ for a two-fluid boundary layer, (a) $\mu_{BT} = 1.0$. (b) $\mu_{BT} = 0.5$. (c) $\mu_{BT} = 0.1$. $Re = 800$. Contour levels correspond to $0 \leq \theta \leq 70$ at an increment of 5. 14

11 Optimum coupling coefficient, θ_{opt} for a two-fluid boundary layer. ——, $d = 0.05$; - - -, $d = 0.1$. $Re = 800$ 14

12 Vertical profiles of streamwise mean velocities at various x-stations. ——, $\mu_{BT} = 1.0$; · · · ·, $\mu_{BT} = 0.5$; — · —, $\mu_{BT} = 0.3$; - - -, $\mu_{BT} = 0.2$. 16

13 Vertical profiles of u_{rms} at various x-stations. ——, $\mu_{BT} = 1.0$; · · · ·, $\mu_{BT} = 0.5$; — · —, $\mu_{BT} = 0.3$; - - -, $\mu_{BT} = 0.2$. 17

14 Maximum u_{rms} versus downstream distance from the inlet plane for (a) the outer fluid and (b) for the entire y-domain. —— $\mu_{BT} = 1$; · · · · $\mu_{BT} = 0.8$; — · — $\mu_{BT} = 0.7$; - - - $\mu_{BT} = 0.5$; —□— $\mu_{BT} = 0.3$; —▽— $\mu_{BT} = 0.2$. 18

15 Instantaneous contours of streamwise velocity fluctuations evaluated at $y/\delta_0 = 0.7$. (a) $\mu_{BT} = 0.7$, (b) $\mu_{BT} = 0.5$, (c) $\mu_{BT} = 0.3$. Contour levels correspond to $-0.002 \leq u \leq 0.002$ at an increment of 0.0004. 18

Summary

Boundary layer stability, and the ability to maintain a laminar flow near the wall, are compromised in presence of free-stream vortical forcing. The low-frequency free-stream disturbances penetrate boundary layer despite the sheltering ability of the mean shear. These disturbances form streaks via the lift-up mechanism. The streaks subsequently become unstable and breakdown to turbulence. The stability of laminar boundary layers is examined in presence of a thin wall-film, of different viscosity. The influence of the film on the evolution of free-stream vortical modes and the generation of boundary layer streaks is solved analytically. It is shown that a lower viscosity film can reduce the transient amplification due to the lift-up mechanism, and hence enhance the flow stability. However, the presence of the wall-film also introduces a new mechanism for the generation of normal vorticity. This mechanism become dominant when the viscosity of the lower film is reduced below a critical level. The results from the linear analysis are complemented by direct numerical simulations which take into account non-parallel and non-linear effects, e.g. finite displacement of the two-fluid interface.

1. Introduction

The mechanics of two-fluid shear flows are significant in many engineering and aerodynamical applications. For example, the instability of two-fluid flows affects the aerodynamic lift of airfoils in the presence of deicing agents, and the heat transfer rates in sheared-films in cooling flows. Here, the influence of a different viscosity film near the wall on boundary layer transition is investigated.

In single-fluid boundary layers, the mean shear limits the penetration of vortical disturbances towards the wall. This inviscid phenomenon is known as *shear-sheltering*. The presence of viscosity, however, renders the sheltering mechanism less effective, and vortical disturbances permeate the shear. As such, laminar boundary layers become prone to bypass transition even at moderate levels of free-stream turbulence (Morkovin 1969). In this report, we focus on the effect of introducing a thin wall film, with respect to the penetration of free-stream vortical disturbances towards the wall. The starting point of our study is the continuous spectrum eigenmodes of the Orr–Sommerfeld equation – the linear perturbation equation for parallel shear flow. The dependence of mode shape on wavenumber, mean shear, and fluid properties demonstrate the influence the wall film on vortical penetration into the boundary layer.

1.1. *The continuous spectrum*

The first formal mathematical characterization of the continuous spectrum, and the analytical expression of its dispersion relation, were presented by Grosch & Salwen (1978). The eigenfunctions of the continuous spectrum are oscillatory in the free-stream, and decay inside the boundary layer shear, as they approach the wall. An example of Orr–Sommerfeld continuous modes, with different frequency, is shown in figure 1.1. The varying degree of penetration, therefore, provides a link between the free-stream turbulence spectrum and the mean shear. Penetration is a function of the perturbation wavenumber (in all three directions) and the flow properties. Figure 1.1 shows the effect of the temporal frequency of the mode. Penetration in increased as the modal frequency is reduced (while the wall-normal and spanwise wavenumbers are held fixed).

When a wall film is introduced, the extent of modal penetration becomes a function of the film viscosity. A sample eigenfunction of the continuous modes for two-fluid boundary

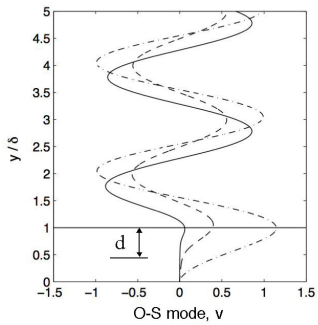

FIGURE 1. Effect of ω on penetration depth ($R = 1000, k_z = \pi, k_y = \pi$) , ——— $\omega = \pi$, - - - $\omega = \pi/10$, —·— $\omega = \pi/100$.

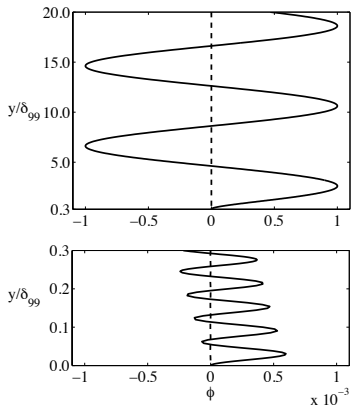

FIGURE 2. High frequency oscillations in mode shape for an extremely dense film. ———, real component; - - -, imaginary component. $k_x Re_T = 1/100, k_y = \pi/4, k_z = \pi, \delta_B = 0.3, \rho_{BT} = 1000$. Note, ϕ is plotted on separate scales in the top and bottom fluids

layers is shown in figure 2. The figure demonstrates that a low-viscosity film changes the wall-normal wavenumber of the vortical mode, inside the film region. The scale-conversion mechanism can enhance penetration of the vortical mode at low viscosity. This result, by Zaki & Saha (2009) defies the accepted, or common, wisdom regarding shear sheltering.

In order to provide a quantitative measure of sheltering, Zaki & Saha (2009) defined the penetration depth,

$$d \equiv \int_0^{\delta_{BL}} \frac{|\phi|}{|\phi|_\infty}\, dy,$$

where $|\phi|_\infty$ is the free-stream amplitude of the eigenfunction. This norm is evaluated over a range of film viscosities, and the results are shown in figure 3. The optimal viscosity ratio, $\nu_{BT}^\star \equiv (\nu_B/\nu_T)^\star$, is clearly shown. As the viscosity ratio is increased, the bottom fluid is essentially an impenetrable layer and the single-fluid boundary layer results are recovered. In the opposite limit, where the bottom fluid is less viscous, shear sheltering becomes dominant and penetration is suppressed. Therefore, a low-viscosity film best

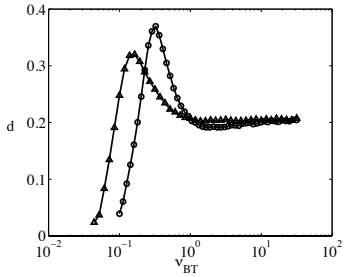

FIGURE 3. Variation of penetration depth with viscosity ratio where $k_x Re_T = \frac{1}{100}, k_y = \frac{\pi}{4}, k_z = \pi$, $\circ$ $\delta_B = 0.3$, $\triangle$ $\delta_B = 0.2$

suited for sheltering the boundary layer from free-stream vortical forcing, and delaying bypass transition.

1.2. *The amplification of streaks*

Beyond the initial stage of boundary layer receptivity to free-stream turbulence, elongated boundary layer streaks are formed and amplify. Their growth has been explained by rapid distortion theory (Phillips 1969), and the *lift-up* mechanism (Landahl 1980). An alternative explanation is provided by the Orr–Sommerfeld and Squire equations for linear perturbations: A three-dimensional, wall-normal v-disturbance tilts the mean vorticity, and thus generates a strong normal vorticity disturbance (Zaki & Durbin 2005, 2006). At low frequencies, the generation of wall-normal vorticity is equivalent to strong streamwise velocity disturbance, or streaks.

Despite the importance of the vorticity tilting mechanism in the amplification of perturbations in a single-fluid boundary layer, it has not been investigated in the context of two-fluid boundary layers. Furthermore, the presence of the interface in a two-fluid boundary layer can lead to interfacial instability mechanisms (Yih 1967; Hooper & Boyd 1983; Hinch 1984; Hooper & Boyd 1987). In this investigation we take advantage of the thin layer effect which stabilizes the interfacial mode, (Renardy 1987; Charru & Hinch 2000) when the film viscosity is lower than the outer stream. The stabilization of the interface mode, however, explains only the large time asymptotic behavior of the system. In studies of transient amplification, even a stable interface mode must be taken into account in evaluating the short time energy amplification.

We herein report on the influence of wall-films of the amplification of streaks forced by free-stream vortical disturbances. Our approach uses the linear perturbation equations. The solution to an initial value problem which governs the boundary layer response is obtained using the eigen-modes of the Orr–Sommerfeld and Squire equations. Thereafter the boundary layer response to low-frequency vortical forcing is evaluated for different viscosities of the wall film. The findings based on linear theory are complemented by direct numerical simulations (DNS). The DNS takes into account non-parallel effects associated with the downstream spreading of the boundary layer. In addition, the DNS also accounts for the finite displacement of the two-fluid interface – a non-linear effect not captured by the linear analysis.

The background to the influence of free-stream vortical modes on boundary layers was presented in this section. The next section, §2, includes the theoretical formulation for the base flow, the governing equations, and the analytical solution of the initial value

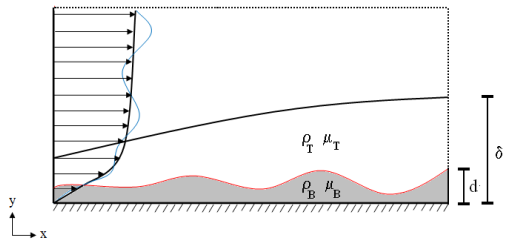

FIGURE 4. Schematic of a two-fluid boundary layer under the influence of a continuous mode and an interface mode.

problem. An example evaluation of the solution of the initial value problem is discussed in §3, and comparison to DNS is given in §4 followed by the conclusion section (§5).

2. Linear analysis

2.1. *The base flow*

The two-fluid boundary layer does not satisfy a similarity solution. Therefore, the boundary layer equations must be marched downstream in order to obtain the correct velocity profile at a given streamwise location. These equations, and their solution procedure, were given in Nelson *et al.* (1995) and are included below:

$$F\partial_\eta^2 F + \nu_j \partial_\eta^3 F - \xi\left(\partial_\eta F \frac{\partial \partial_\eta F}{\partial \xi} - \partial_\eta^2 F \frac{\partial F}{\partial \xi}\right) = 0, \tag{2.1}$$

where $\xi = \left(\frac{U_\infty x}{2\nu_T}\right)^{1/2}$, $\eta = y\left(\frac{U_\infty}{2\nu_T x}\right)^{1/2}$, and $F = \frac{\Psi}{(2\nu_T x U_\infty)^{1/2}}$ with Ψ as the streamfunction. The evolution of the interface η^* is described by the kinematic condition,

$$\frac{\partial \eta^*}{\partial \xi} = \frac{1}{\xi}\left(\frac{V}{U} - \eta^*\right), \tag{2.2}$$

where U and V are the mean streamwise and wall-normal velocities at the interface respectively. The interface boundary conditions are continuity of velocity and stress at $\eta = \eta^*$, according to,

$$[F] = 0 \quad ; \quad [\partial_\eta F] = 0 \quad ; \quad [\mu \partial_\eta^2 F] = 0,$$

where [.] denotes the change across the interface, $(.)_T - (.)_B$. In addition, $F(\xi, \eta)$ must satisfy the boundary conditions,

$$F(\xi, 0) = 0,\ \partial_\eta F(\xi, 0) = 0,\ \lim_{\eta \to \infty} \partial_\eta F(\xi, \eta) = 1.$$

The solution procedure of the above equations follows the description in Schlichting (1987, pp 187-191), and was implemented by Zaki & Saha (2009). This solution provides the mean profile used in the computation of the continuous spectrum modes.

2.2. *The linear perturbation equations*

The evolution of linear perturbations in a parallel shear flow can be fully described by three equations for the normal velocity v, the interface deflection f, and normal-vorticity η. These equations are expressed in operator form according to,

$$\frac{\partial}{\partial t}\begin{pmatrix}\nabla^2 v_j\\ f\\ \eta_j\end{pmatrix} = \begin{pmatrix}\mathscr{L}_j & 0 & 0\\ \mathscr{D} & \mathscr{I} & 0\\ \mathscr{C}_j & 0 & \mathscr{S}_j\end{pmatrix}\begin{pmatrix}v_j\\ f\\ \eta_j\end{pmatrix}.$$

Under the parallel-shear-flow approximation, the equations are homogeneous in time, as well as the streamwise x and spanwise z directions. Therefore, the following form of the solution can be assumed,

$$\begin{pmatrix}v_j\\ f\\ \eta_j\end{pmatrix} = \begin{pmatrix}\hat{\phi}_j(y)\\ \hat{f}\\ \hat{\chi}_j(y)\end{pmatrix} e^{i(k_x x + k_z z - \omega t)}. \tag{2.3}$$

Substituting the normal mode assumption 2.3 in the governing equation 2.3 yields the Orr–Sommerfeld , interface, and Squire eigenvalue problems for two-fluid flows,

$$-i\omega\begin{pmatrix}d_y^2 - k^2 & 0 & 0\\ 0 & 1 & 0\\ 0 & 0 & 1\end{pmatrix}\begin{pmatrix}\hat{\phi}_j(y)\\ \hat{f}\\ \hat{\chi}_j(y)\end{pmatrix} = \begin{pmatrix}\mathscr{L}_j & 0 & 0\\ \int_0^\infty \delta(y-y_f) & \mathscr{I} & 0\\ \mathscr{C}_j & 0 & \mathscr{S}_j\end{pmatrix}\begin{pmatrix}\hat{\phi}_j(y)\\ \hat{f}\\ \hat{\chi}_j(y)\end{pmatrix} \tag{2.4}$$

The operators, $\mathscr{L}_j, \mathscr{I}, \mathscr{C}_j, \mathscr{S}_j$ are defined as,

$$\begin{aligned}
\mathscr{L}_j &= ik_x d_y^2 U_j + \frac{1}{Re_j}(d_y^2 - k^2)^2 - ik_x U_j (d_y^2 - k^2)\\
\mathscr{D}(\bullet) &= \int_0^\infty (\bullet)\delta(y - y_f)dy\\
\mathscr{I} &= -ik_x U(y_f)\\
\mathscr{S}_j &= \frac{1}{Re_j}(d_y^2 - k^2) - ik_x U_j\\
\mathscr{C}_j &= ik_z d_y U_j,
\end{aligned}$$

where $k^2 \equiv k_x^2 + k_z^2$ and $d_y \equiv \frac{d}{dy}$.

Boundary conditions must be enforced at the wall, across the interface, and in the free-stream. The wall and free-stream boundary conditions are similar to the single-fluid case,

$$\hat{\phi}_B(0) = 0; \quad d_y\hat{\phi}_B(0) = 0; \quad \hat{\chi}_B(0) = 0$$
$$\hat{\phi}_T(y\to\infty) = 0;\ d_y\hat{\phi}_T(y\to\infty) = 0;\ \hat{\chi}_T(y\to\infty) = 0.$$

Across the interface, the following conditions of velocity and stress continuity must be

enforced on $\hat{\phi}$ at $y = y_f$,

$$\hat{\phi}_T = \hat{\phi}_B$$
$$d_y\hat{\phi}_T - ik_x d_y U_T \hat{f} = d_y\hat{\phi}_B - ik_x d_y U_B \hat{f}$$
$$\mu_T(d_y^2 + k^2)\hat{\phi}_T - ik_x\mu_T d_y^2 U_T \hat{f} = \mu_B(d_y^2 + k^2)\hat{\phi}_B - ik_x\mu_B d_y^2 U_B \hat{f}$$
$$\rho_T\Big[- i\omega d_y\hat{\phi}_T - Re_j^{-1}\Big(d_y^3 - 3k^2\Big)\hat{\phi}_T + ik_x(U_T d_y\hat{\phi}_T - \hat{\phi}_T d_y U_T)\Big]$$
$$= \rho_B\Big[- i\omega d_y\hat{\phi}_B - Re_j^{-1}\Big(d_y^3 - 3k^2\Big)\hat{\phi}_B + ik_x(U_B d_y\hat{\phi}_B - \hat{\phi}_B d_y U_B)\Big] + We^{-1}k^4\hat{f}.$$

The interfacial conditions on $\hat{\chi}$ are as follows,

$$\hat{\chi}_T - \hat{\chi}_B = -ik_z(d_y U_T - d_y U_B)\hat{f}$$
$$\mu_T d_y\hat{\chi}_T - \mu_B d_y\hat{\chi}_B = ik_z(\mu_T d_y^2 U_T - \mu_B d_y^2 U_B)\hat{f}$$

2.3. *The solution of the initial value problem*

Here, we consider the effect of a vertical velocity, v, perturbation on the two-fluid boundary layer. We prescribe the initial condition for v, and to compute the boundary layer response using the perturbation equations 2.3.

For a general disturbance, we introduce the Fourier transform in the streamwise and the spanwise directions,

$$v_{j,\vec{k}}(y,t) = \int_{-\infty}^{\infty}\int_{-\infty}^{\infty} v_j(\vec{x},t)e^{-ik_x x}e^{-ik_z z}dxdz$$
$$f_{\vec{k}}(t) = \int_{-\infty}^{\infty}\int_{-\infty}^{\infty} f(x,z,t)e^{-ik_x x}e^{-ik_z z}dxdz$$
$$\eta_{j,\vec{k}}(y,t) = \int_{-\infty}^{\infty}\int_{-\infty}^{\infty} \eta_j(\vec{x},t)e^{-ik_x x}e^{-ik_z z}dxdz.$$

The normal velocity and the interface equations form an autonomous sub-system, independent of the normal vorticity. Therefore, this subsystem is solved first. The solution is expressed in terms of the discrete and continuous eigenfunctions of the Orr–Sommerfeld and interface equations. The discrete and continuous spectra, combined, form a complete basis. Therefore, the solution is expanded according to,

$$\begin{pmatrix} v_{\vec{k}}(y,t) \\ f_{\vec{k}}(t) \end{pmatrix} = \sum_{n=1}^{Nos_{\vec{k}}} a_{\vec{k},n}(t)\begin{pmatrix} \hat{\phi}_{\vec{k},n}(y) \\ \hat{f}_{\vec{k},n} \end{pmatrix} + \int_{k_y} a_{\vec{k},k_y}(t)\begin{pmatrix} \hat{\phi}_{\vec{k},k_y}(y) \\ \hat{f}_{\vec{k},k_y} \end{pmatrix} dk_y. \tag{2.5}$$

The orthogonality of the adjoint system is invoked in order to solve for the evolution of the coefficients, $a_{\vec{k},n}$ and $a_{\vec{k},k_y}$. Here, we focus on an initial disturbance that is composed of only a single Orr–Sommerfeld mode,

$$a_{\vec{k},m}(0) = 0 \; a_{\vec{k},k_y}(0) = A\delta(k_y - \tilde{k}_y).$$

Following the procedure in Salwen & Grosch (1981), the following solution is obtained,

$$v_{j,\vec{k}}(y,t) = A\hat{\phi}_{j,\vec{k},\tilde{k}_y}(y)e^{-i\omega_{\vec{k},\tilde{k}_y}t}$$
$$f_{\vec{k}}(t) = A\hat{f}_{\vec{k},\tilde{k}_y}e^{-i\omega_{\vec{k},\tilde{k}_y}t}. \tag{2.6}$$

The Squire equation

Zaki & Durbin (2005) proposed the solution to the forced Squire equation for a single-fluid boundary layer, in terms of the eigenfunctions of the Squire modes. The Squire eigenfunctions, $\hat{\chi}$, satisfy the homogeneous Squire equation,

$$(-i\omega + ik_x U_j)(d_y^2 - k^2)\hat{\chi}_j - \frac{1}{Re_j}(d_y^2 - k^2)\hat{\chi}_j = 0 \tag{2.7}$$

and homogeneous interfacial conditions,

$$\begin{aligned} \hat{\chi}_T - \hat{\chi}_B &= 0 \\ \mu_T d_y \hat{\chi}_T - \mu_B d_y \hat{\chi}_B &= 0. \end{aligned} \tag{2.8}$$

For a two-fluid boundary layer, the homogeneous Squire eigenfunctions remain continuous across the interface. This introduces a difficulty since the normal vorticity we wish to represent is discontinuous at the interface, and must satisfy the following interfacial jump conditions,

$$\eta_{T,\vec{k}}(y_f, t) - \eta_{B,\vec{k}}(y_f, t) = -ik_z\Big(d_y U_T(y_f) - d_y U_B(y_f)\Big) f_{\vec{k}}(t),$$

$$\mu_T \partial_y \eta_{T,\vec{k}}(y_f, t) - \mu_B \partial_y \eta_{B,\vec{k}}(y_f, t) = -ik_z\Big(\mu_T d_y^2 U_T(y_f) - \mu_B d_y^2 U_B(y_f)\Big) f_{\vec{k}}(t).$$

In order to satisfy the above jump conditions implicitly, a change of variables is introduced. The new variable Ψ is continuous and defined as,

$$\Psi_{j,\vec{k}}(y, t) \equiv \eta_{j,\vec{k}}(y, t) + ik_z d_y U_j f_{\vec{k}}(t) g(y). \tag{2.9}$$

The function $g(y)$ must be continuous and differentiable over the interval $[0, \infty)$ for Ψ to be continuous and satisfy the interfacial jump conditions. Moreover $g(y)$ should equal unity at the interface and zero at the wall. The choice of $g(y)$ does not affect our results and any $g(y)$ which satisfies the above conditions can serve the purpose of solving the initial value problem. In this particular case, we use $g(y) = \frac{y}{y_f} e^{y_f - y}$. Thus the interfacial boundary conditions on Ψ are identical to those on the eigenfunctions $\hat{\chi}$,

$$\begin{aligned} \Psi_{T,\vec{k}}(y_f, t) - \Psi_{B,\vec{k}}(y_f, t) &= 0 \\ \mu_T \partial_y \Psi_{T,\vec{k}}(y_f, t) - \mu_B \partial_y \Psi_{B,\vec{k}}(y_f, t) &= 0. \end{aligned}$$

Substituting definition 2.9 into the Squire equation yields the evolution equation for Ψ,

$$\frac{\partial}{\partial t}\Psi_{j,\vec{k}}(y, t) - \mathscr{S}_j \Psi_{j,\vec{k}}(y, t) = \mathscr{F}_j e^{-i\omega_{\vec{k},\tilde{k}_y} t}, \tag{2.10}$$

where the forcing term $\mathscr{F}_j$ is,

$$\mathscr{F}_j = -ik_z A\Bigg[\, d_y U_j \Big(\hat{\phi}_{j,\vec{k},\tilde{k}_y}(y) - \hat{\phi}_{j,\vec{k},\tilde{k}_y}(y_f) g(y)\Big) + Re_j^{-1}\left(d_y^2 - k^2\right)\Big(d_y U_j g(y)\Big) f_{\vec{k},\tilde{k}_y}\Bigg].$$

Following Zaki & Durbin (2005), we expand Ψ in terms of the homogeneous Squire eigenfunctions,

$$\Psi_{\vec{k}}(y, t) = \sum_{m=1}^{Nsq_{\vec{k}}} b_{\vec{k},m}(t)\hat{\chi}_{\vec{k},m}(y) + \int_{k_y} b_{\vec{k},k_y}(t)\hat{\chi}_{\vec{k},k_y}(y) dk_y. \tag{2.11}$$

The amplitude functions, $b_{\vec{k},m}(t)$ and $b_{\vec{k},k_y}(t)$ can be derived using the bi-orthogonality

condition satisfied by the adjoint Squire eigenfunctions. Following a similar procedure as outline in Zaki & Durbin (2005) yields the evolution equations for the spectral coefficients,

$$\begin{aligned}\frac{d}{dt}b_{\vec{k},m}(t) &= -i\omega_{\vec{k},n}b_{\vec{k},n}(t) + \langle\hat{\chi}^{\dagger}_{\vec{k},m},\mathscr{F}_j\rangle e^{-i\omega_{\vec{k},\tilde{k}_y}t}\\ \frac{d}{dt}b_{\vec{k},k_y}(t) &= -i\omega_{\vec{k},k_y}b_{\vec{k},k_y}(t) + \langle\hat{\chi}^{\dagger}_{\vec{k},k_y},\mathscr{F}_j\rangle e^{-i\omega_{\vec{k},\tilde{k}_y}t}\end{aligned} \tag{2.12}$$

Equation 2.12 is a first order, ordinary differential equation and can be solved exactly for the amplitude functions,

$$b_{\vec{k},m}(t) = b_{\vec{k},m}(0)e^{-i\omega_{\vec{k},m}t} - \langle\hat{\chi}^{\dagger}_{\vec{k},m},\mathscr{F}_j\rangle\left[\frac{e^{-i\omega_{\vec{k},\tilde{k}_y}t} - e^{-i\omega_{\vec{k},m}t}}{i\omega_{\vec{k},\tilde{k}_y} - i\omega_{\vec{k},m}}\right]$$

Since the continuous spectrum of the Squire and the Orr–Sommerfeld equation overlap, there exists a continuous Squire mode which resonates with the forcing Orr–Sommerfeld mode. Therefore, for the resonant mode, $k_y = \tilde{k}_y$, the amplitude is given by

$$b_{\vec{k},k_y}(t) = b_{\vec{k},k_y}(0)e^{-i\omega_{\vec{k},k_y}t} - \langle\hat{\chi}^{\dagger}_{\vec{k},k_y},\mathscr{F}_j\rangle t\left[e^{-i\omega_{\vec{k},\tilde{k}_y}t}\right], \tag{2.13}$$

and for non-resonant Squire modes $k_y \neq \tilde{k}_y$

$$b_{\vec{k},k_y}(t) = b_{\vec{k},k_y}(0)e^{-i\omega_{\vec{k},k_y}t} - \langle\hat{\chi}^{\dagger}_{\vec{k},k_y},\mathscr{F}_j\rangle\left[\frac{e^{-i\omega_{\vec{k},\tilde{k}_y}t} - e^{-i\omega_{\vec{k},k_y}t}}{i\omega_{\vec{k},\tilde{k}_y} - i\omega_{\vec{k},k_y}}\right].$$

Finally, the normal vorticity η is recovered from Ψ using equation 2.9.

3. Evaluation of the boundary layer response to vortical forcing

Although the solution to the initial value problem is general, our objective is to evaluate the effect of viscosity stratification on a two-fluid boundary layer. Therefore, surface tension effects are ignored, and we assume unit density ratio. Focus is placed on studying the two-fluid boundary layer response to an initial forcing by a streamwise oriented vortex. This type of forcing is known to be most effective at generating streaks in the single-fluid problem. Furthermore, the initial condition assumes zero interface displacement. This condition is constructed from a superposition of an O-S mode with finite interfacial displacement and an interface mode.

The continuous Orr–Sommerfeld mode resonantly forces Squire equation, and the solution 2.13 explicitly demonstrates initial algebraic growth with time for the resonant Squire eigenmode. The inner product, $|\langle\hat{\chi}^{\dagger}_{\vec{k},k_y},\mathscr{F}\rangle|$ is shown in figure 5, for forcing by (i) the continuous Orr–Sommerfeld mode and (ii) the interface mode. The peak in the projection is at the resonant Squire mode, and hence algebraic transient growth is expected in the response.

The normal velocity profile is shown in figure 6(a) at various times. It is oscillatory in the free-stream and decays inside the boundary layer similar to the single-fluid case. The entire normal velocity field decays with time owing to viscous dissipation. At large times there is no vertical velocity present because the continuous Orr–Sommerfeld mode is exponentially stable, and there is no vertical velocity perturbation associated with the interface mode.

The time evolution of the interface displacement is shown in figure 6(b), and can be

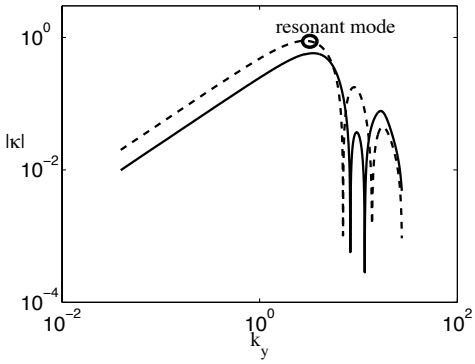

FIGURE 5. Projection of forcing $|\kappa| \equiv |\langle \hat{\chi}^{\dagger}_{\vec{k},k_y}, \mathscr{F} \rangle|$ on the homogeneous Squire eigenfunctions. ——, interfacial mode; - - -, continuous Orr–Sommerfeld mode. The forcing mode has $\omega_{int} = 0.000373$, $k_x = 0.001$, $k_{y,cont} = \pi$, $k_z = \pi$ and the Reynolds number is $Re = 800$. The film thickness and viscosity are $d = 0.1$ and $\mu_{BT} = 0.3$.

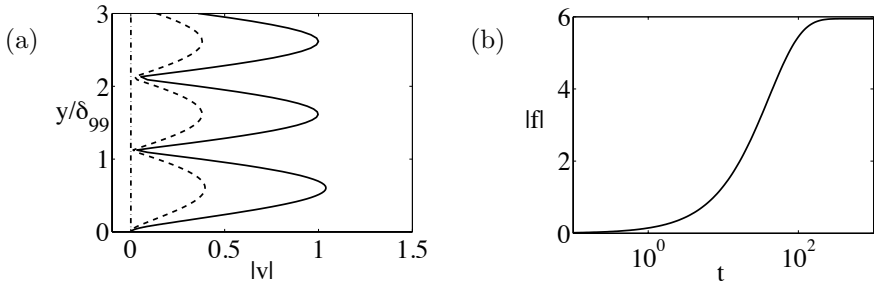

FIGURE 6. (a) Normal velocity and (b) interface displacement at different instants of time. ——, $t = 0$; - - -, $t = 44$; —·—, $t = 314$. The forcing mode has $\omega_{int} = 0.000373$, $k_x = 0.001$, $k_{y,cont} = \pi$, $k_z = \pi$ and the Reynolds number is $Re = 800$. The film thickness and viscosity are $d = 0.1$ and $\mu_{BT} = 0.3$.

explained by examining equation 3.1,

$$f_{\vec{k}}(t) = A_{\vec{k},\tilde{k}_y} f_{\vec{k},\tilde{k}_y} e^{-i\omega_{\vec{k},\tilde{k}_y} t} + A_{\vec{k},int} f_{\vec{k},int} e^{-i\omega_{\vec{k},int} t}. \tag{3.1}$$

The two amplitudes $A_{\vec{k},\tilde{k}_y}$ and $A_{\vec{k},int}$ in equation 3.1 were chosen such that the initial interface displacement is zero. However this cancellation is no longer maintained at larger times since the continuous Orr–Sommerfeld mode decays much faster than the interfacial mode. The net interface displacement therefore increases in time. At large times, only the interface mode is present and therefore interfacial displacement should decay as $e^{-i\omega_{\vec{k},int} t}$.

Figure 7(a) shows the normal vorticity response as a result of the forcing by the interfacial and continuous Orr–Sommerfeld mode. The free-stream solution is trivial at all instants of time. Normal vorticity is generated by the vorticity tilting mechanism, whereby the normal velocity component of the perturbation tilts the mean shear and generates perturbation vorticity. Since there is no mean shear in the free-stream, no normal vorticity is generated. However inside the boundary layer, the normal vorticity perturbation amplifies due to the vorticity tilting mechanism.

Viscous decay sets in on a time-scale, $t_{viscous} \sim O(Re/(k_x^2 + k_y^2 + k_z^2))$. At larger times, the normal velocity perturbation vanishes, and the normal vorticity equation is

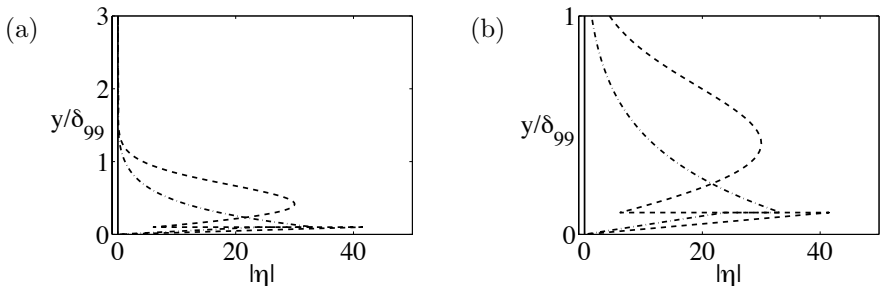

FIGURE 7. (a) Normal vorticity response at different instants in time, ——, $t = 0$; - - -, $t = 44$; —·—, $t = 314$. A zoomed in view of the boundary layer is shown in pane (b). The forcing mode parameters are $\omega_{int} = 0.000373$, $k_x = 0.001$, $k_{y,cont} = \pi$, $k_z = \pi$ and the Reynolds number is $Re = 800$. The film thickness and viscosity are $d = 0.1$ and $\mu_{BT} = 0.3$.

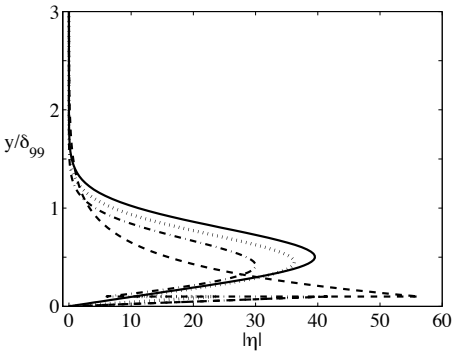

FIGURE 8. Squire response in a two-fluid boundary layer at the time of maximum amplification in energy. $d = 0.1$ ——, $\mu_{BT} = 1.0$; ····, $\mu_{BT} = 0.5$; —·—, $\mu_{BT} = 0.3$; - - -, $\mu_{BT} = 0.2$. $k_x = 0.001, k_y = \pi, k_z = \pi, Re = 800$

driven purely by the displacement of the interface. In the long-time limit, a jump in normal vorticity is observed across the interface and the vorticity perturbation decays away from the interface, as shown in figure 7(b). The large-time normal vorticity field is identical to the particular vorticity associated with the interface mode.

3.1. *Viscosity stratification effects*

A reduction in viscosity ratio, μ_{BT}, increases the amplitude of the interface mode and hence the neutral interfacial wave generates large amplitude normal vorticity. The effect of viscosity stratification on the vorticity tilting mechanism must also be evaluated. Figure 8 shows the Squire response at the time of maximum amplification. The peak in normal vorticity response associated with the vorticity tilting mechanism reduces as the viscosity ratio μ_{BT} is reduced. The forcing term, which is shown in figure 9(a-b) is also attenuated. Therefore, it can be concluded that the temporal amplification due to the vorticity tilting mechanism is reduced by lowering of μ_{BT}.

The origin of the two peaks in normal vorticity has been addressed; the first maximum is due to the tilting of mean vorticity and the second is associated with the neutral interfacial wave. The first peak is therefore dependent on the strength of the forcing term, $\mathscr{C}$ (Zaki & Durbin 2005). This term is affected by the mean shear distribution

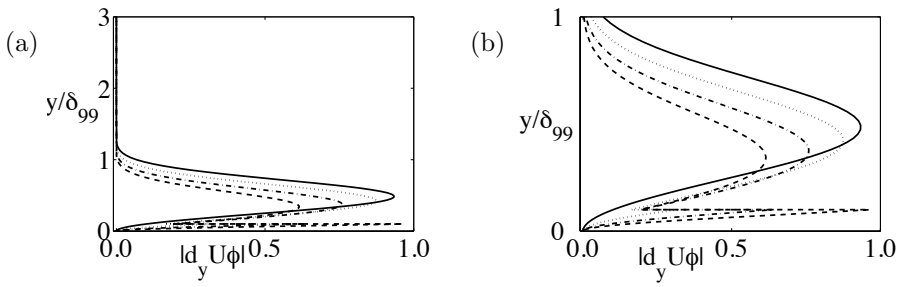

FIGURE 9. (a)Tilting term, $|d_y U\phi|$ for a two-fluid boundary layer (b) Tilting term, $|d_y U\phi|$ inside the boundary layer. $d = 0.1$ ——, $\mu_{BT} = 1.0$; · · · ·, $\mu_{BT} = 0.5$; —— · ——, $\mu_{BT} = 0.3$; - - -, $\mu_{BT} = 0.2$. $k_x = 0.001, k_y = \pi, k_z = \pi, Re = 800$.

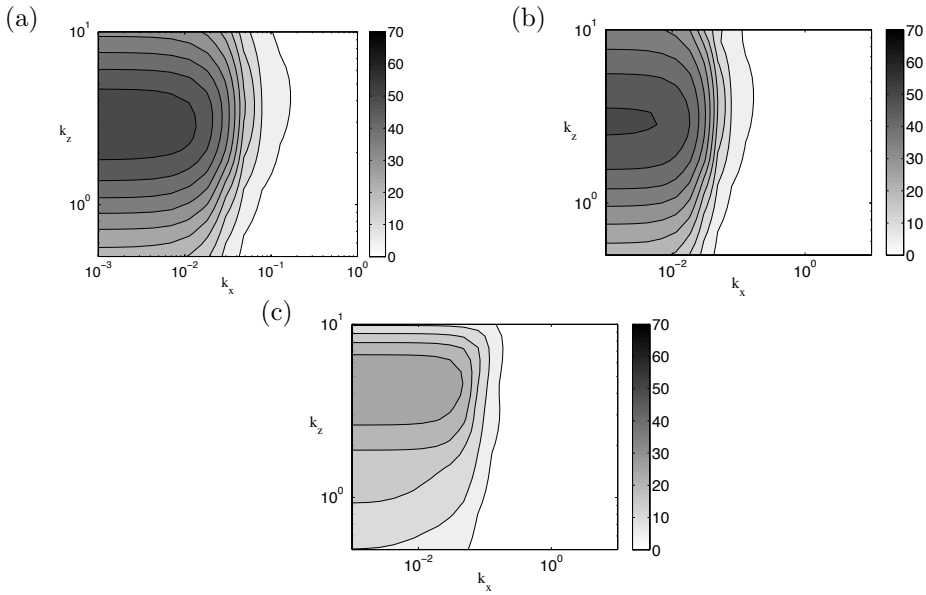

FIGURE 10. Coupling coefficient contours, θ for a two-fluid boundary layer, (a) $\mu_{BT} = 1.0$. (b) $\mu_{BT} = 0.5$. (c) $\mu_{BT} = 0.1$. $Re = 800$. Contour levels correspond to $0 \leq \theta \leq 70$ at an increment of 5.

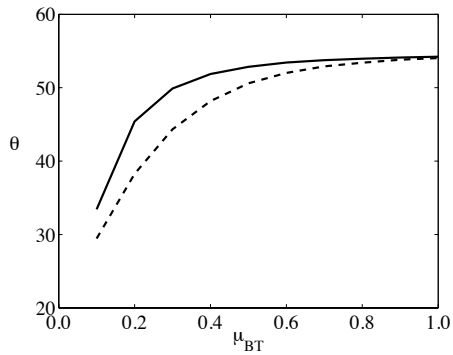

FIGURE 11. Optimum coupling coefficient, θ_{opt} for a two-fluid boundary layer. ——, $d = 0.05$; - - -, $d = 0.1$. $Re = 800$

and the variation in $\hat{\phi}$ with viscosity stratification. As μ_{BT} is reduced, the shear in the bottom fluid increases and the shear in the top fluid is reduced in order to maintain the mean shear stress continuity at the interface. The shape of $\hat{\phi}$ in a two-fluid boundary layer was discussed in detail in the work of Zaki & Saha (2009). It was reported that the penetration of normal velocity perturbation into the boundary layer is inhibited for low viscosity ratios due to the presence of stronger shear in the bottom fluid. Therefore the overall forcing term $\mathscr{C}$ is reduced in strength as the viscosity ratio is reduced. The coupling coefficient $\theta \equiv \left|\frac{\langle \hat{\chi}^{\dagger}, \mathscr{C}\hat{\phi}\rangle}{\omega_i}\right|$ proposed by Zaki & Durbin (2005) was computed, and is shown in figures 10(a-c). As the viscosity ratio is reduced, the optimum coupling coefficient is significantly reduced compared to the single-fluid value.

Below a critical viscosity ratio, the neutral interfacial wave generates normal vorticity which exceeds the mean-vorticity tilting mechanism. For a given viscosity ratio a thicker film absorbs the mean shear to a greater extent and therefore the coupling between mean shear and normal velocity is weaker. This implies that the vorticity tilting mechanism is expected to be weaker for a thicker film. This prediction is substantiated by figure 11 which shows the coupling coefficient optimized over all k_x, k_y and k_z. The optimal θ is larger for the thinner film.

The solution to the initial value problem indicates that the temporal amplification of streaks is reduced in presence of low-viscisoty wall film. The equivalent spatial problem is now studied using direct numerical simulations. In the next section, the numerical method used in our direct numerical simulations is introduced, followed by a discussion of the results from our direct computations.

4. Direct numerical simulations

Direct numerical simulations (DNS) take into account the downstream spreading of the base flow, and non-linear effects such as the finite displacement of the interface between the two fluids. These phenomena were not modelled in the linear analyses above. Non-parallel effects can play an important role because the free-stream vortical forcing of interest is low-frequency. Therefore, the mean flow spreading with distance from the leading edge effects the boundary layer response to these elongated modes. With regards to non-linear effects, finite displacement of the interface can change the effective amplification rate of disturbances Cheung & Zaki (2010), and ultimately change in the interface topology Cheung & Zaki (2011). These effects have modelled herein using direct solutions of the Navier-Stokes equations, and the two-fluid interface is simulated using a mass-conserving interface-capturing scheme.

In order to compare the DNS results to linear theory, the numerical simulations are performed at small-amplitude inflow perturbations. A single low-frequency continuous Orr-Sommerfeld mode is prescribed at the inflow of our computational domain, and its spatial evolution is computed for six different viscosity ratios, $\mu_{BT} = \{0.2, 0.3, 0.5, 0.7, 0.8, 1.0\}$. The film-thickness is set to 10% of the boundary layer thickness at the inlet.

4.1. *The numerical method*

The time-dependent Navier-Stokes equations are solved using a fractional step algorithm. A local volume-flux formulation is utilized, on a staggered computational grid in general curvilinear coordinates (Rosenfeld *et al.* 1991). The convective terms are treated explicitly using the Adams-Bashforth scheme. The pressure and diffusion terms are treated

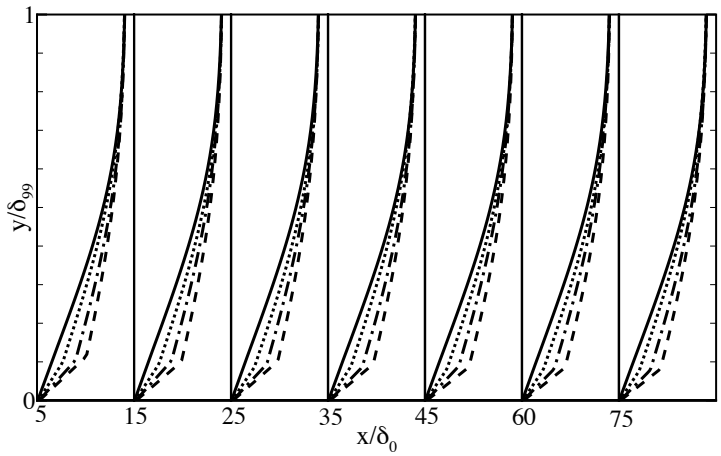

FIGURE 12. Vertical profiles of streamwise mean velocities at various x-stations. ——, $\mu_{BT} = 1.0$; ····, $\mu_{BT} = 0.5$; —·—, $\mu_{BT} = 0.3$; - - -, $\mu_{BT} = 0.2$.

by implicit Euler method, and by Crank-Nicolson method, respectively. This code is parallelized using Message Passing Interface (MPI).

The inflow to the computational domain is a superposition of the two-fluid boundary layer profile, and a single mode perturbation. The inlet Reynolds number is $Re_{\delta_0} = 800$, based on the inlet boundary-layer thickness and free-stream velocity. The streamwise, wall-normal and spanwise sizes of the computational domain are, $L_x/\delta_0 = 300$, $L_y/\delta_0 = 20$ and $L_z/\delta_0 = 8$, respectively. The number of grid points used is (N_x, N_y, N_z)=$(257, 129, 65)$. The grid is uniformly spaced in the streamwise x and spanwise z directions, and is clustered near the interface in the wall-normlal y direction. The height of the computational domain is selected to be sufficiently large in order to ensure that the boundary layer is unaffected by the far field boundary conditions. The convective outflow condition is applied at the exit plain. A no-slip boundary condition is imposed at the solid wall. In the free stream, the following boundary conditions are enforced, $u = U_\infty$ and $\frac{\partial v}{\partial y} = \frac{\partial w}{\partial y} = 0$. Periodicity is enforced in the spanwise direction. For the single-mode perturbation, the inflow mode is $\omega = 0.01$, $k_y = \pi$, $k_z = \pi$, and the amplitude of the inflow disturbance is normalized such that $v_{rms} = 0.01\%$ in the free stream.

The two-fluid interface is represented by an iso-surface, or a level-set of a smooth function. The conventional level-set technique uses the signed distance function. However, this approach yields poor mass conservation. Therefore, the current work adopts the conservative level-set method in conjunction with a ghost fluid approach (Desjardins *et al.* 2008). This method ensures accurate and robust interface transport by using a hyperbolic tangent level set function. Moreover, the sharp discontinuity of the interface can be captured by the ghost fluid method.

4.2. *Numerical results*

The influence of the viscosity ratio on the mean velocities is shown in figure 12. Here, the y-axis is normalized by the local boundary layer thickness and four different viscosity ratios are plotted. It is clearly seen that the wall film absorbs the mean shear and this tendency is more pronounced with decreasing viscosity of the film. As a result, it is

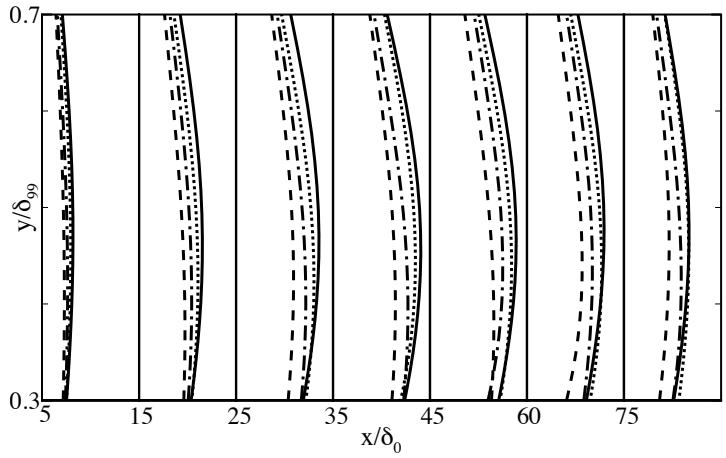

FIGURE 13. Vertical profiles of u_{rms} at various x-stations. ——, $\mu_{BT} = 1.0$; · · · ·, $\mu_{BT} = 0.5$; — · —, $\mu_{BT} = 0.3$; - - -, $\mu_{BT} = 0.2$.

expected that the lift-up mechanism will be weaker for a less viscous film, since the mean mean shear is decreased in the top fluid as shown in figure 9.

The root-mean-square (rms) streamwise velocity fluctuations at different x-locations are displayed in figure 13. The wall-normal axis is shown in the range $0.3 < y/\delta_{99} < 0.7$, outside the wall film, in order to demonstrate the attenuation of the streak clearly. The streamwise velocity fluctuations for $\mu_{BT} = 1.0$ are increasing from the inlet to $x/\delta_0 \approx 45$ and then decay as they convect further downstream. This trend is also observed for other viscosity ratios. The boundary layer streaks are most amplified at $x/\delta_0 \approx 45$, which is very close to the time of maximum amplification predicted by the linear analysis. Furthermore, the streak amplitude becomes weaker with decreasing viscosity ratio. This is consistent with the linear prediction that lower viscosity wall films attenuate the energy amplification inside the boundary layer.

The maximum u_{rms} is extracted at every downstream location and is plotted in figure 14. In figure 14(a), the maximum is computed from the disturbance field in the outer fluid, and therefore reflects the strength of the streaks in the outer stream due to tilting of mean vorticity. The maximum values of the u_{rms} for the streaks are located at $x/\delta_0 \approx 40$. This peak amplification decreases at lower viscosity ratios, which is consistent with the prediction of linear theory. The relative decrease in the maximum u_{rms} is as large as 30% for the lowest viscosity ratio, $\mu_{BT} = 0.2$. It should be noted in figure 14(b), however, that the maximum values of u_{rms} for $\mu_{BT} = 0.2$ and 0.3 are significantly higher than those of other viscosity ratios and the maxima show slow decay rates for $x/\delta_0 > 100$. This indicates that the inflow disturbances decay much faster than the u-perturbation induced by the interfacial mechanism, as explained by linear theory.

Plan views of the instantaneous streamwise velocity fluctuations are shown in figure 15. The figure also affirms the reduction of the streak strength by a lower-viscosity wall-film. The solution to the initial value problem presented earlier neglects both non-parallel and nonlinear effects. Here, the base-flow spreading and the interfacial displacement are fully represented, but the amplitude of the disturbance was kept small in order to

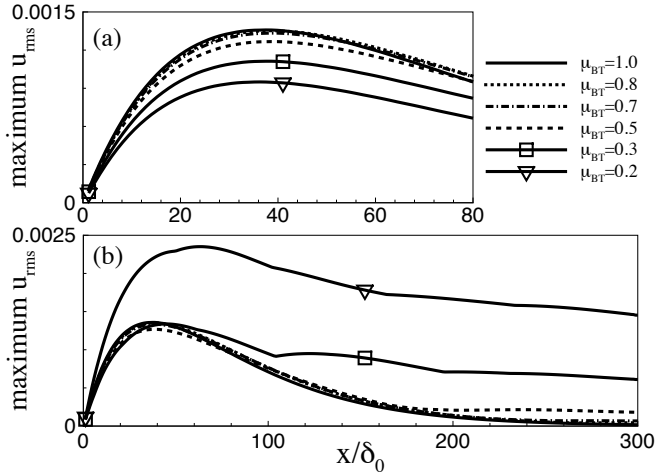

FIGURE 14. Maximum u_{rms} versus downstream distance from the inlet plane for (a) the outer fluid and (b) for the entire y-domain. —— $\mu_{BT} = 1$; ···· $\mu_{BT} = 0.8$; —·— $\mu_{BT} = 0.7$; - - - $\mu_{BT} = 0.5$; —□— $\mu_{BT} = 0.3$; —▽— $\mu_{BT} = 0.2$.

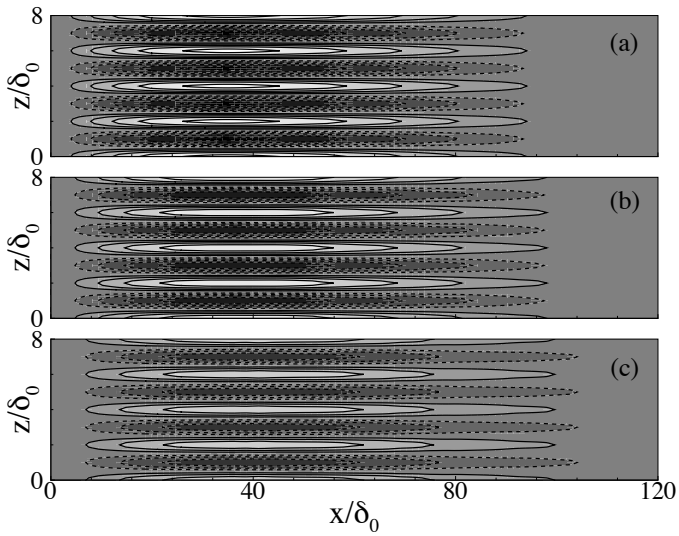

FIGURE 15. Instantaneous contours of streamwise velocity fluctuations evaluated at $y/\delta_0 = 0.7$. (a) $\mu_{BT} = 0.7$, (b) $\mu_{BT} = 0.5$, (c) $\mu_{BT} = 0.3$. Contour levels correspond to $-0.002 \leq u \leq 0.002$ at an increment of 0.0004.

preserve linear behavior. The agreement between the DNS and linear theory therefore complements the analyses presented herein.

5. Conclusions

The amplification of streaks, due to low-frequency vortical disturbances has been investigated in two-fluid boundary layers. The presence of a different viscosity wall-film influences (i) the penetration of vortical disturbances into the mean shear and (ii) and the amplification of the boundary layer response. The latter was studied by solving the

initial value problem of normal-vorticity generation (Squire response) by vertical-velocity forcing (O–S mode). The analytical solution shows that the presence of a low-viscosity wall-film can weaken the lift-up mechanism. This is due to the redistribution of the mean shear, which becomes concentrated near the wall, where the vertical velocity is vanishingly small. This explanation was supported by evaluation of the coupling coefficient between the O–S forcing and the Squire response. The coefficient affirmed that the reduction in viscosity ratio yields weaker streaks in the context of the lift-up mechanism. However, the presence of a viscosity mismatch at the interface introduces another source of normal vorticity. The interface deformation also forces the Squire equation, and can lead to normal-vorticity response, although at a longer time scale.

The linear analyses, while shed light on the linear mechanism of streak amplification, do not address (a) non-paralllelism in the base flow and (b) non-linear effects such as the finite deformation of the interface. The former is important because the streaks are streamwise elongated structures, and can therefore be sensitive to the downstream spreading of the boundary layer. Since the interface displacement is finite, and Klebanoff streaks reach high amplitude, non-linear effects can be appreciable. In order to address non-parallelism of the base flow and non-linear effects due to the interface movement, direct numerical simulations were carried out, albeit for low-amplitude disturbances. An accurate, conservative level-set approach was used in order to track the evolution of the interface, and the boundary layer response to particular vortical modes. The results were consistent with the prediction of linear theory: the outer streaks were weaker in the presence of low-viscosity wall film. In addition, a near-interface peak in u-perturbation was observed due to the interface deformation mechanism. This peak increased with lower film viscosity, and acted on a longer time-scale than the well-known lift-up mechanism.

REFERENCES

Charru, F. & Hinch, E. J. 2000 'Phase diagram' of interfacial instabilities in a two-layer Couette flow and mechanism of the long-wave instability. *Journal of Fluid Mechanics* **414**, 195–223.

Cheung, L. C. & Zaki, T. A. 2010 Linear and nonlinear instability waves in spatially developing two-phase mixing layers. *Physics of Fluids* **22** (052103).

Cheung, L. C. & Zaki, T. A. 2011 A nonlinear pse method for two-fluid shear flows with complex interfacial topology. *Journal of Computational Physics* .

Desjardins, O., Moureau, V. & Pitsch, H. 2008 An accurate conservative level set/ghost fluid method for simulating turbulent atomization. *Journal of Computational Physics* **227**, 8395–8416.

Grosch, C. E. & Salwen, H. 1978 The continuous spectrum of the Orr-Sommerfeld equation. Part 1. The spectrum and the eigenfunctions. *Journal of Fluid Mechanics* **87**, 33–54.

Hinch, E. J. 1984 A note on the mechanism of the instability at the interface between two shearing fluids. *Journal of Fluid Mechanics* **144**, 463–465.

Hooper, A. P. & Boyd, W. G. C. 1983 Shear-flow instability at the interface between viscous fluids. *Journal of Fluid Mechanics* **128**, 507–528.

Hooper, A. P. & Boyd, W. G. C. 1987 Shear-flow instability due to a wall and a viscosity discontinuity at the interface. *Journal of Fluid Mechanics* **179**, 201–225.

Landahl, M. T. 1980 A note on an algebraic instability of inviscid parallel shear flows. *Journal of Fluid Mechanics* **98**, 243–251.

Morkovin, M. V. 1969 *Viscous Drag Reduction*, chap. On the many faces of transition. Plenum.

Nelson, J. J., Alving, A. E. & Joseph, D. D. 1995 Boundary layer flow of air over water on a flat plate. *Journal of Fluid Mechanics* **284**, 159–169.

Phillips, O. M. 1969 Shear-flow turbulence. *Annual Review of Fluid Mechanics* **1**, 245–264.

Renardy, Y. 1987 The thin-layer effect and interfacial stability in a two-layer Couette flow with similar liquids. *Physics of Fluids* **30** (6), 1627–1637.

Rosenfeld, M., Kwak, D. & Vinokur, M. 1991 A fractional step solution method for the unsteady incompressible Navier–Stokes equations in generalized coordinate systems. a fractional step solution method for the unsteady incompressible Navier–Stokes equations in generalized coordinate systems. *Journal of Computational Physics* **94**, 102–137.

Salwen, H. & Grosch, C. E. 1981 The continuous spectrum of the Orr-Sommerfeld equation. Part 2. Eigenfunction expansions. *Journal of Fluid Mechanics* **104**, 445–465.

Schlichting, H. 1987 *Boundary-Layer Theory*, 7th edn. McGraw-Hill.

Yih, C. S. 1967 Instability due to viscosity stratification. *Journal of Fluid Mechanics* **27**, 337–352.

Zaki, T. A. & Durbin, P. A. 2005 Mode interaction and the bypass route to transition. *Journal of Fluid Mechanics* **531**, 85–111.

Zaki, T. A. & Durbin, P. A. 2006 Continuous mode transition and the effects of pressure gradient. *Journal of Fluid Mechanics* **563**, 357–388.

Zaki, T. A. & Saha, S. 2009 On shear sheltering and the structure of vortical modes in single and two-fluid boundary layers. *Journal of Fluid Mechanics* **626**, 113 – 148.